TR－A－0109

Static Analysis of Posture and Movement, Using a 17-muscle Model of the Monkey's Arm

Menashe DORNAY

1991. 3.29

ATR視聴覚機構研究所

〒619-02 京都府相楽郡精華町乾谷 ☎07749-5-1411

ATR Auditory and Visual Perception Research Laboratories

Inuidani, Seika-cho, Soraku-gun, Kyoto 619-02 Japan

Telephone: +81-7749-5-1411
Facsimile: +81-7749-5-1408
Telex: 5452-516 ATR J

Static Analysis of Posture and Movement, Using a 17-muscle Model of the Monkey's Arm

Menashe DORNAY
Cognitive Processes Department,
ATR Auditory and Visual Perception Research Laboratories,
Sanpeidani, Inuidani, Seika-cho, Soraku-gun, Kyoto 619-02, JAPAN.

ABSTRACT

The musculo skeletal apparatus of the arm transforms motor commands via muscle forces into joint torques. A stable equilibrium posture with zero net force at the hand is specified when the joint stiffness is stable, and the net joint torque is zero. **The transformation from a stable spring-like muscle space into joint and hand space can potentially induce hand postural instability.**

In this study I show kinematic and static constraints of the neuro-musculo-skeletal arm of the monkey which are needed for the postural stability of the hand. My results enhance the previously proposed impedance control theory, and present new aspects for controlling the hand stiffness. A new term, **the angular stiffness of individual muscles**, is introduced. Using muscles with varying moment-arms, I show that while individual muscles may have unstable angular stiffness, only the summation of the angular stiffnesses of the individual muscles determines the joint (and hand) postural stability.

A computer model of the arm, based on biological measurements, with 17 muscles, is shown. The model is used to determine the effect of a given muscle activation patterns on the posture and stability of the hand.

Using the equilibrium point hypothesis, arm movement is modeled as a gradual shift of a stable equilibrium posture of the hand along a desired trajectory. Given initial and final equilibrium postures of the hand, and using a minimum potential energy change constraint, the simulator derives the motor commands to the muscles for creating the desired trajectory.

1. INTRODUCTION

The broad purpose of this work is to study, in a kinematic and static approach, the way in which the primate central nervous system (CNS) maintains the hand at a desired posture, and how it controls the movement of the hand.

The hand is at an equilibrium position when its velocity is zero, no external force acts on it, and the net internal force at the hand, produced by the muscles, is zero. The postural stability of the hand is shown when it is displaced by a small transient external disturbance from an equilibrium position. It is characterized by a restoring force generated by the muscles for returning the hand to its original position. The postural stability was shown both in the absence and presence of feedback (Bizzi et al. 1986; Feldman 1986; Mussa-Ivaldi et al. 1985; Taub et al. 1975). Modeling muscles as tunable elastic elements led to the development of the equilibrium point hypothesis (EP) for the control of posture and movement (Bizzi et al. 1986; Feldman 1966, 1986; Hogan 1985). These observations suggested that postural stability results from the CNS coordinating the activity levels of agonist and antagonist muscles around a joint. When the torque due to the flexor muscles around a joint T_f, cancels the torque due to the extensors T_e, an equilibrium position is defined for that joint (Fig. 1). An estimate for evaluating the stability of a planar "spring-like" hand was proposed using its **symmetric** stiffness matrix (Fig. 1).

$$\mathbf{K} = \frac{\partial \mathbf{F}}{\partial \mathbf{X}} = \begin{bmatrix} \frac{\partial F_x}{\partial x} & \frac{\partial F_x}{\partial y} \\ \frac{\partial F_y}{\partial x} & \frac{\partial F_y}{\partial y} \end{bmatrix} = \begin{matrix} hand \\ stiff \\ -ness \end{matrix} \quad \mathbf{F} = \begin{bmatrix} F_x \\ F_y \end{bmatrix} = \begin{matrix} hand \\ force \end{matrix} \quad \mathbf{X} = \begin{bmatrix} x \\ y \end{bmatrix} = \begin{matrix} hand \\ position \end{matrix} \qquad (1)$$

The hand equilibrium position is stable if and only if all the eigenvalues of the hand stiffness have a negative real part (Ogata, 1970). In our case the eigenvalues must be real and not complex (Johnson et al. 1989) because $\mathbf{K}$ is a $n \times n$ real symmetric matrix (Mussa-Ivaldi et al. 1985).

2. ILL-POSED MOTOR-CONTROL PROBLEMS

Voluntary-movement control is an ill-posed rather than well-posed problem. A problem is well-posed when its solution exists, is unique and depends continuously on the initial data. Ill-posed problems fail to satisfy one or more of these criteria. Most motor-control problems are ill-posed in the sense that their solution is not unique.

In a classical set of experiments, Bizzi et al. (1982, 1984) showed that arm movements, both in intact and deafferented monkeys, consist of a gradual shift of the hand along a set of intermediate stable equilibrium positions while the hand moves from the

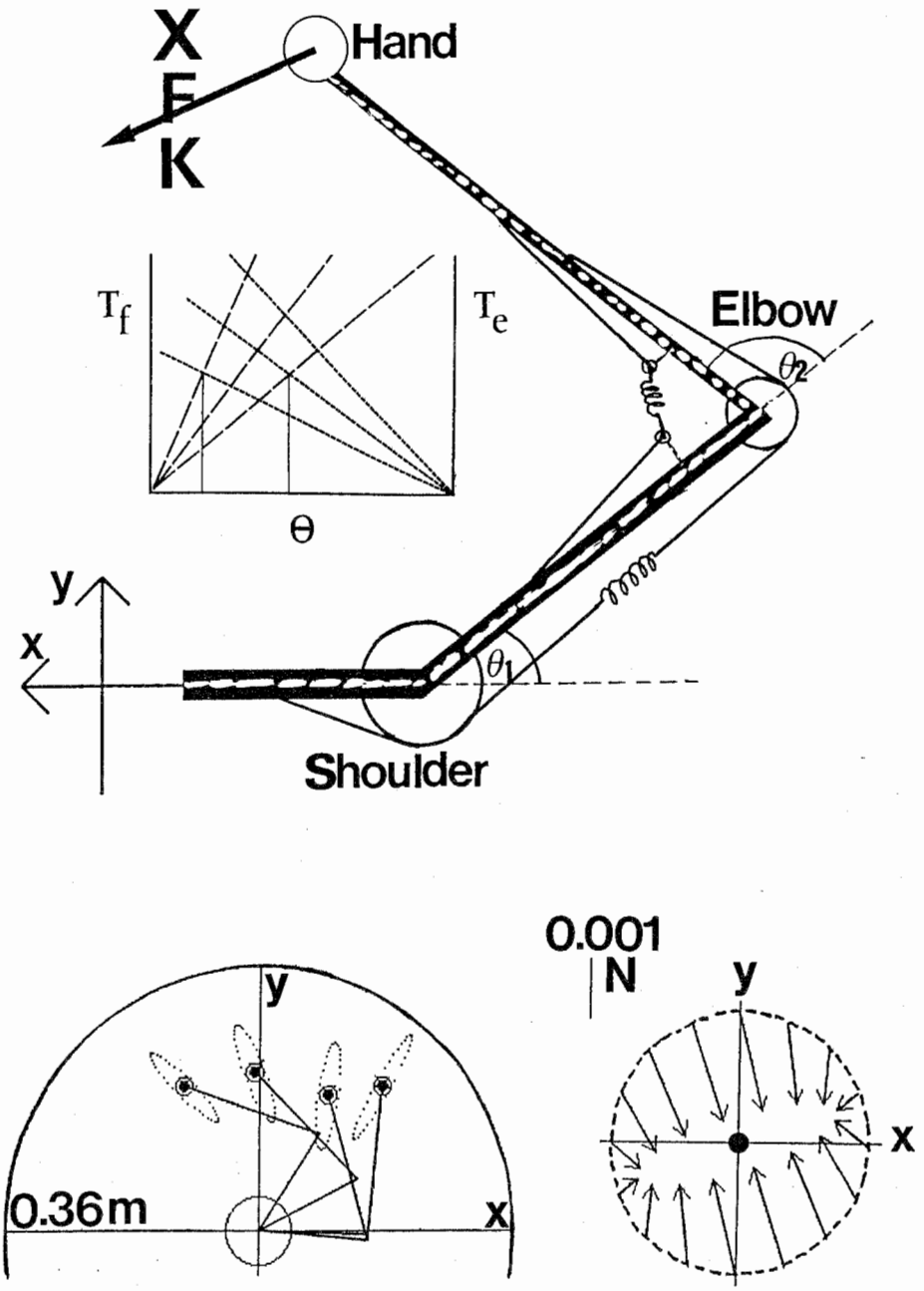

Fig. 1. A schematic planar 2-joint arm model. **Top:** One double joint extensor and an elbow single joint flexor muscles are shown. An equilibrium position for a joint is specified when the torque due to the flexor muscles around that joint T_f, cancels the torque due to the extensors T_e. When both joints are at equilibrium the force at the hand, **F**, is zero, and the hand is also at equilibrium. **Bottom-left:** When the hand is displaced from a **stable** equilibrium position, an elastic restoring force is observed. Plotting the magnitudes of the restoring forces, following $0.01\times10^{-2}m$ displacements around the equilibrium position, as a distance from the equilibrium position, creates stiffness ellipses. **Bottom-right** Typical directions and relative magnitudes of the restoring forces at $0.01\times10^{-2}m$ displacements from the equilibrium position of the hand. The directions of the restoring forces are not necessarily towards the equilibrium position. The stiffnesses data were obtained from the monkey-arm simulator, described in this paper. The stiffness representation was proposed by Mussa-Ivaldi et al. 1985.

initial to the target position. The equilibrium point hypothesis (EP) is very attractive because its unified treatment of posture and movement is consistent with these experiments.

The EP cannot by itself control arm movement, because no tools are specified for solving the following ill-posed problems: (A) Which trajectory (hand path and velocity) should be used while moving the hand. (B) Given a solution to (A), what motor commands should the muscles receive to specify each intermediate state of the hand while it is moving. Solutions to problem (A), the **minimum-jerk model**, and to problem (B) the **backdriving algorithm** were proposed (Flash and Hogan 1985; Mussa-Ivaldi et al. in press).

The minimum-jerk model estimates the smoothest hand trajectory during movement. Assuming that the movement starts and ends with zero hand velocity and acceleration, the minimum-jerk model predicts a straight hand path with a bell-shaped velocity profile. These predictions are in good agreements for unconstrained point to point hand movements in the horizontal plane in front of the body (Flash 1987; Morasso 1981; Uno et al. 1989).

The backdriving algorithm implements the experimental evidence (Bizzi et al. 1982, 1984) and the EP by modeling arm movements as a gradual shift of the hand along a set of stable intermediate equilibrium points from the initial to the final hand positions. Moving the hand from one intermediate point to another during movement is done by an active change in the motor commands to the muscles.

The ill-posed problem of finding the new motor commands to the muscles is solved by a pseudo-inverse which minimizes the change in potential energy stored in the muscles, while creating the driving motor commands to move the hand from one intermediate point to the next.

In this work I use the minimum-jerk model to create the hand trajectory, and the backdriving algorithm to predict the motor commands to the muscles.

3. A PLANAR 2-JOINT ARM MODEL

A planar 2-joint model of the arm is shown in Fig. 1. The torso, upperarm, and forearm links are modeled as rigid one dimensional line segments, representing the bones. The 3 links are interconnected by the shoulder and elbow revolute joints. The relative angles of rotation are $\theta_1 \in [-45^o, 90^o]$ for the shoulder and $\theta_2 \in [30^o, 135^o]$ for the elbow. Link lengthes, attachment centers on the bones and volumes of the muscles were measured by anatomical dissections in 2 rhesus monkeys. A total of seventeen muscles including shoulder, elbow and two-joint flexors and extensors have been included in the model (Table 1, Dornay et al. 1989; Dornay 1990, 1991).

An adult rhesus monkey (Macaca mulatta) whose weight was 9.86 Kg was used for the 1st dissection, after being sacrificed and perfused through its heart with $4\times10^{-3}\ m^3$ of saline solution (0.9 % NaCl water solution). The muscles listed in Table 1 were

TABLE 1, THE DISSECTED MUSCLES.

#	Muscle	Origin	Insertion	Function
1	Latissimus Dorsi	Vertebrae	Humerus	Shoulder Extensor
2	Posterior Deltoid	Scapula	Humerus	Shoulder Extensor
3	Teres-Major	Scapula	Humerus	Shoulder Extensor
4	Teres-Minor	Scapula	Humerus	Shoulder Extensor
5	Infra-Spinatus	Scapula	Humerus	Shoulder Extensor
6	Pectoralis Major Capsularis	Clavicula	Humerus	Shoulder Flexor
7	Pectoralis Major Sternalis	Sternum	Humerus	Shoulder Flexor
8	Anterior Deltoid	Clavicula	Humerus	Shoulder Flexor
9	Coraco Brachialis	Scapula	Humerus	Shoulder Flexor
10	Triceps Lateralis	Humerus	Ulna	Elbow Extensor
11	Triceps Medialis	Humerus	Ulna	Elbow Extensor
12	Brachialis	Humerus	Ulna	Elbow Flexor
13	Brachio-Radialis	Humerus	Radius	Elbow Flexor
14	Pronator Teres	Humerus	Radius	Elbow Flexor
15	Triceps Longus	Scapula	Ulna	2-Joint Extensor
16	Biceps Brevis	Scapula	Radius	2-Joint Flexor
17	Biceps Longus	Scapula	Radius	2-Joint Flexor

exposed and their centers of attachments were marked by drilling metal screws into the bones. The volumes of the muscles were measured by water displacements. The monkey skeleton was cleaned and reassembled to a configuration similar to the one used by alive monkeys (Bizzi et al. 1986) during experimental horizontal arm movements (Fig. 2).

Planar projection of the 3-dimensional skeleton was done by x-ray analysis (Fig. 3). The lengthes of the upperarm and forearm links were measured to be 15.5×10^{-2} and 20.2×10^{-2} m respectively (Fig. 3). The coordinates of the centers of attachments of the muscles on the bones were measured from the planar projection of the x-ray (Fig. 3), and confirmed by using standard textbooks (Hartman and Straus, 1933; Berringer et al. 1968; Gray 1959). A second dissection on another adult rhesus monkey was done to confirm qualitatively the coordinates of attachments of the muscles to the bones. In the second dissection the same 17 muscles were removed and their volumes were measured serving as duplicates to the results obtained from the 1st dissection. Each volume of the muscles obtained in the second dissection was scaled by the total volume of the muscles from the 1st dissection divided by the total volume of the muscles from the 2nd dissection. After scaling, the difference between duplicate volumes obtained for each muscle were less than 10%. Table 2 summarizes the average volumes and the coordinates of attachment of the muscles.

Each muscle is modeled as either a straight line, or partially a straight line and partially a curved line wrapped around its individual pulley(s) at the joint(s). As an example, the geometry of the shoulder flexor muscle pectoralis major capsularis is shown in Fig. 4A. The radii of the pulleys around the joints were estimated, based on the x-ray analysis, to be $1.0\times10^{-2}m$ for the shoulder flexors and extensors and for the elbow flexors. The radii of the pulleys for the elbow extensors were estimated to be $1.5\times10^{-2}m$.

One of the more prominent features of muscle behavior is the increase of output steady-state force which accompanies both an increase in its length or an increase in its neural input. The length and motor-command dependence of muscle force gives the muscle a behavior analogous to that of a **tunable mechanical spring**. Analysis of the static isometric length-force curves reported for deafferented cat preparation (Rack and Westbury 1969) or intact monkeys (Zeffiro 1986) showed that static muscle forces can be estimated using the following linear equation:

$$f = \kappa(u)\left[l(\theta)-l_0(u)\right] = \begin{matrix} muscle \\ force \end{matrix} \qquad u \in \left[0,\ 1\right] = neural\ \ control\ \ input \tag{2}$$

The motor command u can have any value from zero to one. $\kappa(u)$ is the **negative** muscle stiffness (δf opposes δl), $l(\theta)$ is the length, and $l_0(u)$ is the rest-length (length when $f = 0$). A bigger motor command will increase κ and decrease l_0,

THE MONKEY SKELETON:
A: Ventral view. **B:** Dorsal view.

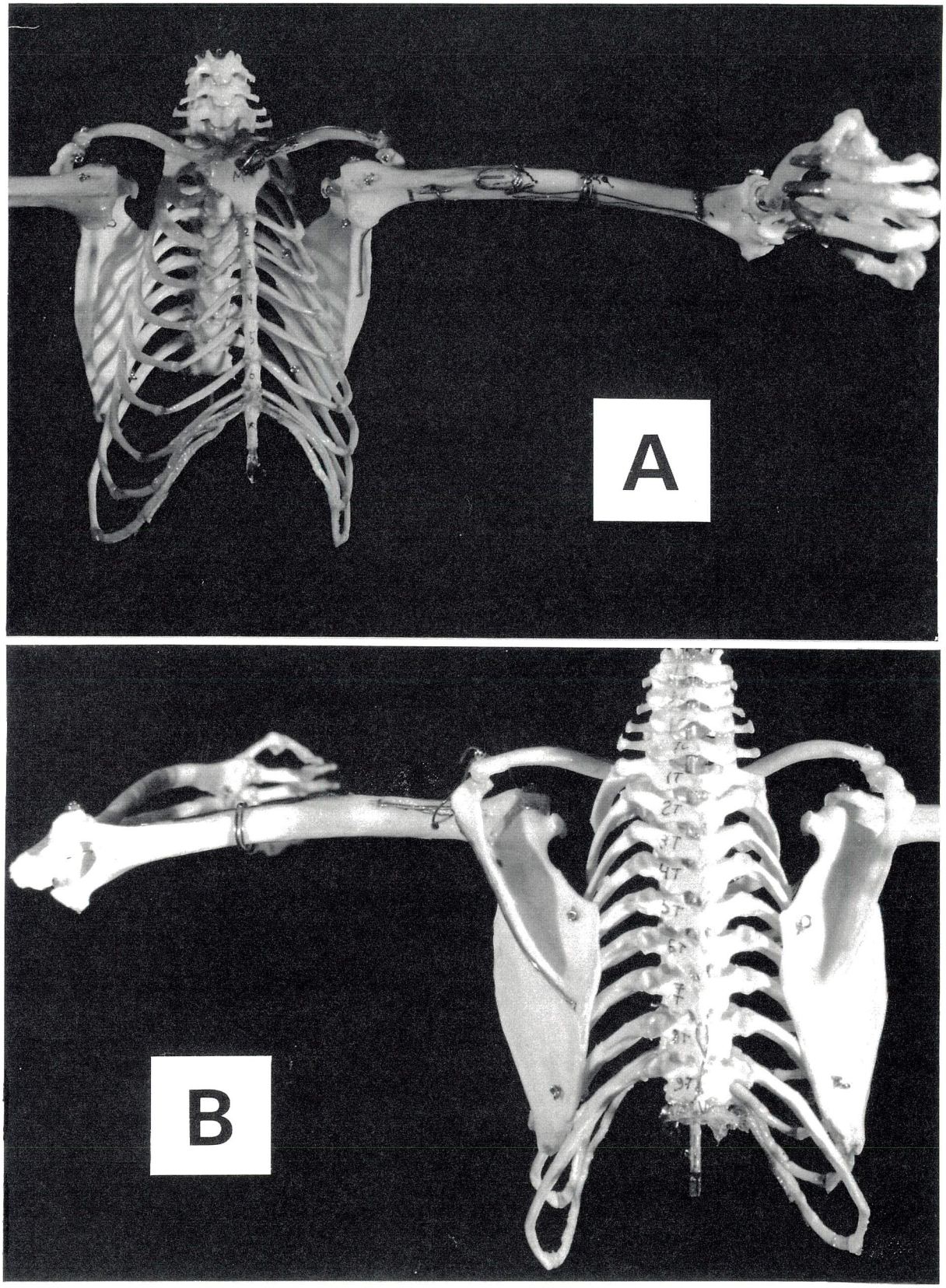

Fig. 2. The monkey skeleton. After cleaning, the skeleton of the monkey was reassembled to a configuration similar to the one used by alive monkeys (Bizzi et al. 1986) during experimental horizontal arm movements.

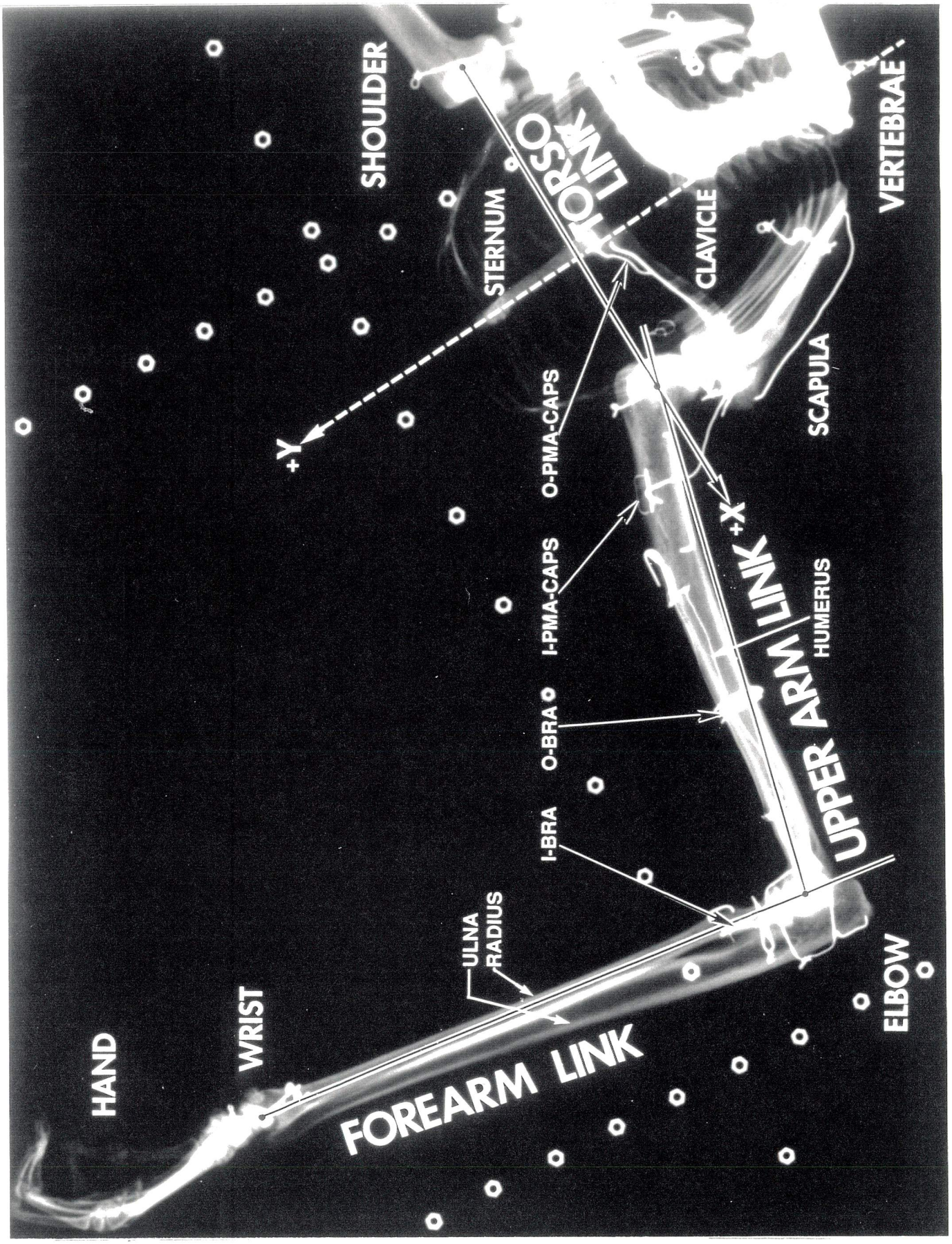

Fig. 3. X-ray analysis. The attachments of the muscles were marked on the skeleton of the monkey. X-ray analysis gave a planar model of the 3-dimensional geometry. The shoulder and elbow joints were modeled as frictionless revolute joints. The torso link is an imaginary line segment connecting the 2 shoulders. The upperarm link is a line connecting the shoulder and elbow joints. The forearm link is the line passing from the elbow through the wrist till the center of the hand.

TABLE 2, GEOMETRY AND VOLUMES OF THE MUSCLES

	Muscle	Origin ($m \times 10^{-2}$)	Insertion ($m \times 10^{-2}$)	Volume ($m^3 \times 10^{-6}$)
1	Latissimus Dorsi	(-5.5, -10.0)	(2.1, 1.0)	50.0
2	Posterior Deltoid	(0.8, -4.4)	(5.2, 1.5)	21.3
3	Teres-Major	(-0.2, -6.4)	(2.8, 0.5)	25.3
4	Teres-Minor	(0.2, -5.0)	(0.8, 0.6)	4.75
5	Infra-Spinatus	(-0.2, -4.8)	(0.8, 0.6)	26.4
6	Pectoralis Major Capsularis	(-4.8, -0.8)	(2.7, 1.5)	37.0
7	Pectoralis Major Sternalis	(-5.5, 1.3)	(2.7, 1.5)	33.0
8	Anterior Deltoid	(-2.4, -2.0)	(5.2, 1.5)	15.1
9	Coraco Brachialis	(-1.6, -1.0)	(6.0, 1.5)	4.3
10	Triceps Lateralis	(-12.2, 0.2)	(-0.8, -1.6)	45.8
11	Triceps Medialis	(-5.6, -0.2)	(-0.8, -1.6)	26.5
12	Brachialis	(-5.7, 0.7)	(2.3, -0.3)	15.2
13	Brachio-Radialis	(-5.0, -0.2)	(16.5, 0.8)	24.4
14	Pronator Teres	(-1.2, -0.5)	(9.3, 0.3)	9.5
15	Triceps Longus	(0.4, -2.2)	(-0.8, -1.6)	45.8
16	Biceps Brevis	(-1.6, -1.0)	(2.7, 0.5)	28.0
17	Biceps Longus	(-0.73, -1.5)	(2.7, 0.5)	26.5

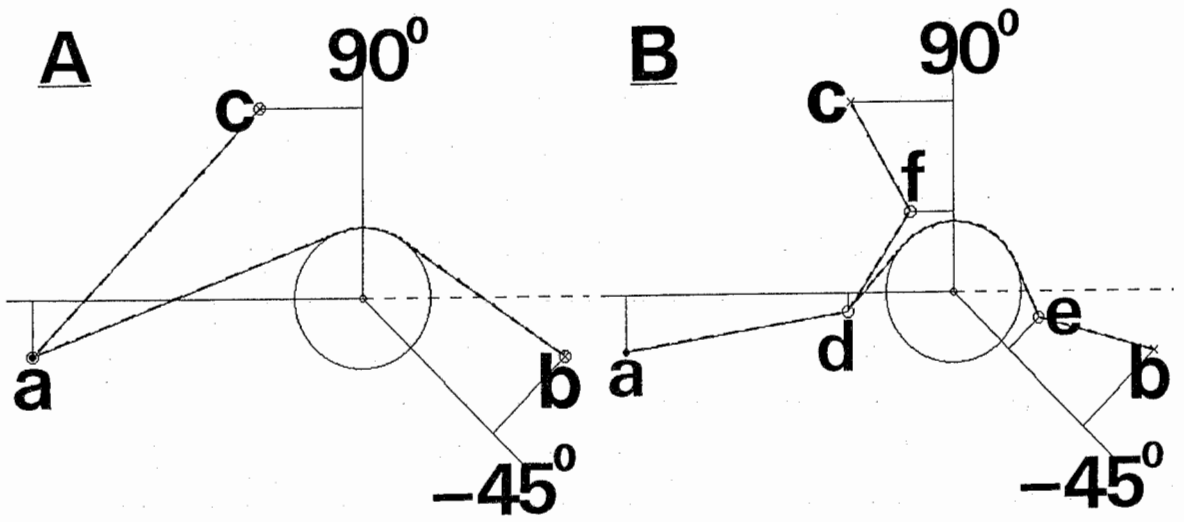

Fig. 4. Geometric models of the shoulder flexor muscle pectoralis major capsularis. **(A) Initial Model:** The muscle originates from the torso link at **a**. The insertion of the muscle to the upperarm link is marked as **b** ($\theta = -45^{o}$) or **c** ($\theta = 90^{o}$). The joint angle affects muscle length and whether it is wrapped around its pulley at the joint (**b**) or is unwrapped (**c**). **(B) Stabilized Model:** The muscle is constrained by connective tissues represented by the effective origin **d** and the effective insertion **e** or **f**. Appendix C describes the heuristic approach which was used to estimate the effective origins and insertions.

increasing the produced muscle force.

Based on those findings, each muscle is represented in this work as an elastic element whose rest-length and stiffness are regulated by a motor command, using the above equation. Measured volumes and estimated rest-lengthes were used as scaling factors, based on in vivo parameters of the triceps which served as a reference muscle (Zeffiro, 1986). A simplified physiological cross-section area (An et al. 1981), used for muscle stiffness scaling, was calculated by dividing the measured muscle volumes by their rest length. Appendix A gives more details on the estimation of muscle stiffnesses and rest-lengthes.

A computer model of the arm was created in object oriented Lisp. An early version of the software, containing both a forward arm model and the backdriving algorithm (McIntyre et al. 1989), was further developed. Based on the developed software, and the biological measurements, a planar model of the monkey's arm, with 17 muscles, was created (Dornay et al. 1989; Dornay 1990, 1991). Modeling muscles as tunable elastic elements, any set of motor commands to the muscles gives a simple well-posed solution for muscle forces, joint torques, hand position and hand force. The equilibrium position of the arm, where the force produced by the hand is zero, corresponds to a configuration in which the potential energy stored by the muscles is at minimum. The backdriving algorithm, described before, was implemented to simulate planar hand movements.

4. INITIAL HAND STABILITY AND MOVEMENTS

Computer simulations revealed that the hand was stable, and movement could be simulated, only in a small portion of the workspace (Fig. 5). The inability to simulate movements was related to postural instability of the hand. (The backdriving algorithm depends on the hand stability, and cannot operate when either of the two eigenvalues of the stiffness of the hand is not negative).

5. HAND STABILITY AND JOINT STIFFNESS

A necessary and sufficient condition for hand stability at equilibrium (F = 0) is that the joint stiffness R is stable. To show it I will use, following Hogan, 1985 and McIntyre, 1990:

$$\mathbf{R} = \begin{bmatrix} \frac{\partial T_1}{\partial \theta_1} & \frac{\partial T_1}{\partial \theta_2} \\ \frac{\partial T_2}{\partial \theta_1} & \frac{\partial T_2}{\partial \theta_2} \end{bmatrix} = \begin{matrix} joint \\ stiffness \end{matrix} \qquad \theta = \begin{bmatrix} \theta_1 \\ \theta_2 \end{bmatrix} = \begin{matrix} joint \\ angle \end{matrix} \qquad \mathbf{T} = \begin{bmatrix} T_1 \\ T_2 \end{bmatrix} = \begin{matrix} joint \\ torque \end{matrix} \qquad (3)$$

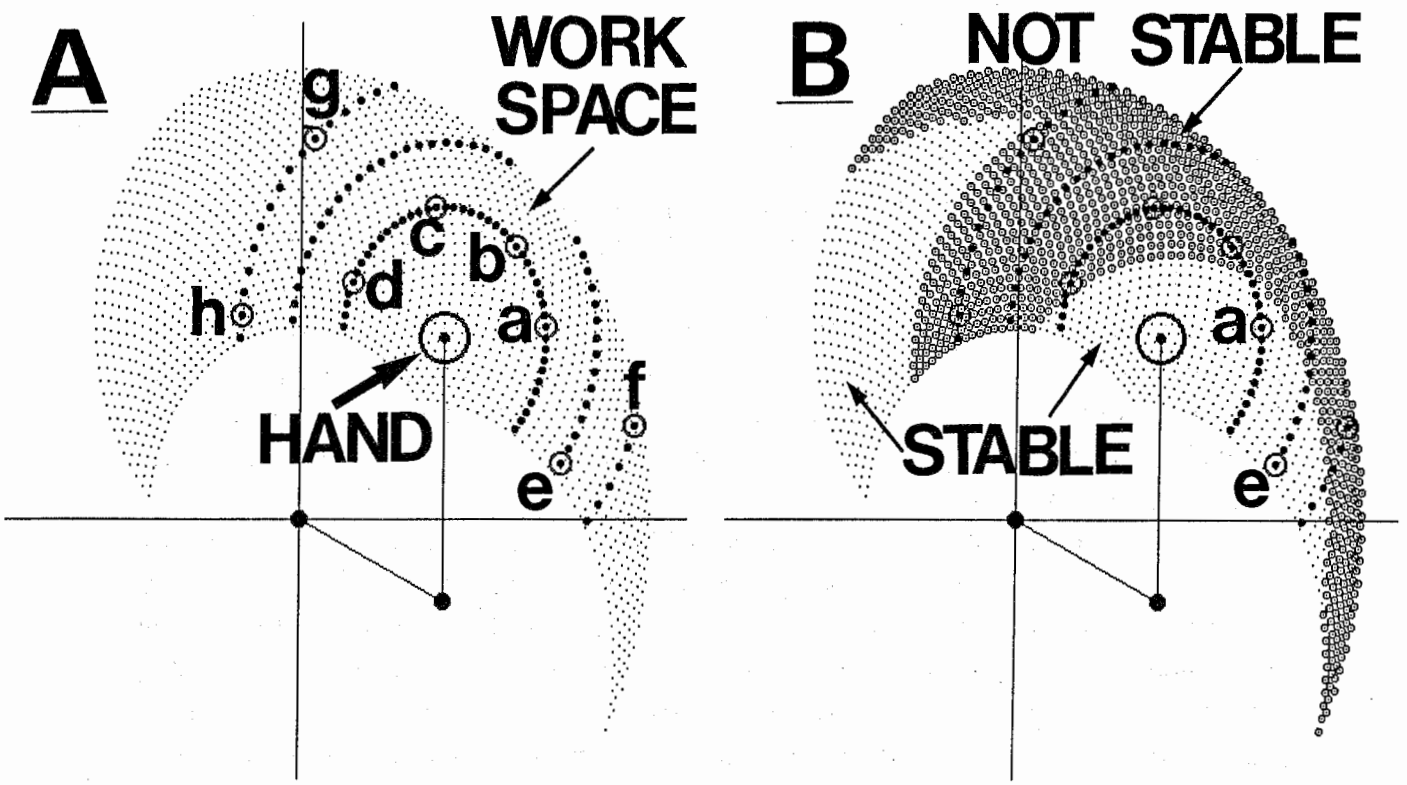

Fig. 5. Initial hand stability. **A:** When the control input to each muscle was 0.5, the hand was stable at the equilibrium position (0.14, 0.14) m. This equilibrium position was used as a center for 0.10, 0.15 and 0.20 m radius circles in the hand workspace. Using the backdriving algorithm, the hand could be moved to points **a** and **e**, but not to points **b**, **c**, **d**, **f**, **g**, **h**. The failure was because the hand stiffness was unstable during these movements. **B:** Superimposing the areas where the joint stiffness is unstable on the previous figure. The control input to each muscle was 0.5. Increasing or decreasing the control input to each muscle to 1.0 or to 0.0 increased or decreased respectively the area in which the joint stiffness was unstable.

$$\mathbf{J} = \frac{\partial \mathbf{X}}{\partial \boldsymbol{\theta}} = \begin{bmatrix} \frac{\partial x}{\partial \theta_1} & \frac{\partial x}{\partial \theta_2} \\ \frac{\partial y}{\partial \theta_1} & \frac{\partial y}{\partial \theta_2} \end{bmatrix} \tag{4}$$

J is the jacobian transformation matrix from joint angle to hand coordinates.

Using $\mathbf{K} = \frac{\partial \mathbf{F}}{\partial \mathbf{X}} = \frac{\partial \mathbf{F}}{\partial \boldsymbol{\theta}} \frac{\partial \boldsymbol{\theta}}{\partial \mathbf{X}} = \frac{\partial \mathbf{F}}{\partial \boldsymbol{\theta}} \mathbf{J}^{-1}$

and based on the principle of virtual work which gives $\mathbf{T} = \mathbf{J}^T \mathbf{F}$ (Mussa-Ivaldi 1986), the joint stiffness $\mathbf{R}$ is defined as:

$$\mathbf{R} = \frac{\partial \mathbf{T}}{\partial \boldsymbol{\theta}} = \frac{\partial (\mathbf{J}^T \mathbf{F})}{\partial \boldsymbol{\theta}} = \mathbf{J}^T \frac{\partial \mathbf{F}}{\partial \boldsymbol{\theta}} + \frac{\partial \mathbf{J}^T}{\partial \boldsymbol{\theta}} \mathbf{F}$$

$$\rightarrow \quad \frac{\partial \mathbf{F}}{\partial \boldsymbol{\theta}} = (\mathbf{J}^T)^{-1} \left[\mathbf{R} - \frac{\partial \mathbf{J}^T}{\partial \boldsymbol{\theta}} \mathbf{F} \right]$$

$$\rightarrow \mathbf{K} = (\mathbf{J}^T)^{-1} \left[\mathbf{R} - \frac{\partial \mathbf{J}^T}{\partial \boldsymbol{\theta}} \mathbf{F} \right] \mathbf{J}^{-1}$$

When $\mathbf{F} = 0$ we get:

$$\mathbf{K} = (\mathbf{J}^T)^{-1} \mathbf{R} \mathbf{J}^{-1} = \left[\mathbf{J}^{-1} \right]^T \mathbf{R} \left[\mathbf{J}^{-1} \right] \tag{5}$$

Based on Sylvester's law of inertia, equation (5) shows that when the hand is at equilibrium then a stable stiffness of the joint is a necessary and sufficient condition for a stable stiffness of the hand (Strang 1988; Ogata 1970).

6. CONDITIONS FOR JOINT STABILITY

We assume that $\mathbf{K}$ is symmetric (Mussa-Ivaldi et al. 1985) and therefore $\mathbf{R}$ is also symmetric. Expressing the symmetry of $\mathbf{R}$ by ρ we get

$$\rho = \left[\frac{\partial T_1}{\partial \theta_2} \right] = \left[\frac{\partial T_2}{\partial \theta_1} \right] \rightarrow \mathbf{R} = \begin{bmatrix} R_{1,1} & \rho \\ \rho & R_{2,2} \end{bmatrix} \tag{6}$$

In order for **R** to be stable, we must find the constrains such that the two eigenvalues λ of **R** are negative (Ogata 1970). Assuming (the reasonable assumption, Mussa-Ivaldi et al. 1985) that the reciprocal angular stiffness ρ is smaller in magnitude relative to $R_{1,1}$ or $R_{2,2}$, Appendix B proves that

$$R_{1,1} < 0,\ R_{2,2} < 0, \longleftrightarrow \lambda_{1,2}(\mathbf{R}) < 0 \tag{7}$$

Using these assumptions, we can see that:
A necessary and sufficient condition for a stable joint stiffness is having stable (or negative) shoulder $R_{1,1}$ and elbow $R_{2,2}$ stiffness. It should be emphasized that this finding is not trivial because of the coupling of the joints by the double joint muscles (Hogan 1985).

7. JOINT STABILITY AND MUSCLE ANGULAR STIFFNESS

The contribution of a muscle force to a joint torque is:

$$\tau = \frac{\partial l}{\partial \theta} f = \mu f \tag{8}$$

μ is called the moment-arm of the muscle. The contribution of a muscle to a joint stiffness or **the angular stiffness of a muscle** is defined as:

$$r = \frac{\partial \tau}{\partial \theta} \tag{9}$$

The meaning of the angular stiffness of a muscle is as follows: **(A)** If r is stable (negative) then changing the joint angle by some external torque will create a restoring torque by that muscle which will try to decrease the change in joint angle. **(B)** If r is not stable then changing the joint angle will create a torque by the muscle which will further increase the change in joint angle.

The joint torques and stiffness can be expressed using the contributions of the individual muscles:

$$\mathbf{R} = \begin{bmatrix} \dfrac{\partial\left[\sum_{i=1}^{m}\tau_{1,i}\right]}{\partial\theta_1} & \rho \\ \rho & \dfrac{\partial\left[\sum_{j=1}^{n}\tau_{2,j}\right]}{\partial\theta_2} \end{bmatrix} = \begin{bmatrix} \sum_{i=1}^{m} r_{1,i} & \rho \\ \rho & \sum_{j=1}^{n} r_{2,j} \end{bmatrix} \tag{10}$$

where τ, r contributions of a muscle to a joint torque and angular stiffness, m, n muscles affecting shoulder or elbow.

8. MUSCLES CAN HAVE UNSTABLE ANGULAR STIFFNESS

The general expression of angular stiffness of a muscle around a joint is:

$$r = \frac{\partial\tau}{\partial\theta} = \frac{\partial(\mu f)}{\partial\theta} = \mu\frac{\partial f}{\partial\theta} + \frac{\partial\mu}{\partial\theta}f \tag{11}$$

Defining $\chi = \partial\mu/\partial\theta$ = momvel (a new name introduced in this paper), the angular stiffness of a muscle is:

$$r = \mu\frac{\partial f}{\partial\theta} + \chi f \tag{12}$$

Considering the specific linear force length model used in this study (Eq. 2), we get:

$$r = \kappa\mu^2 + \chi\kappa(l - l_0) \tag{13}$$

Since the muscles themselves are always stable $\kappa < 0$ and muscles cannot push $(l - l_0) > 0$ the term $\kappa\mu^2$ contributes only stability (negative) and the term $\chi\kappa(l - l_0)$ can become unstable, depending only on χ. This shows that

A necessary condition for unstable angular stiffness of a muscle is that its momvel χ is negative.

When a muscle have unstable angular stiffness,

$$\kappa\mu^2 + \chi\kappa(l - l_0) > 0 \quad \longleftrightarrow \quad \mu^2(\theta) + \chi(\theta)\,[l(\theta) - l_0(u)] < 0 \tag{14}$$

In this case, increasing the control motor command u by the CNS will decrease $l_0(u)$ without any effect on μ, χ or l, making the angular stiffness of that muscle even more unstable.

As a typical example, stability analysis of the shoulder flexor pectoralis major capsularis, whose geometry was shown in Fig. 4A, is shown in Fig. 6.

An intuitive meaning of muscle angular stability can be gained by considering Figs. 4A and 6, in which pectoralis major capsularis is undergoing a flexion from a very extended position. Let us suppose that during this flexion movement the joint as a whole is always at stable equilibrium positions due to the contributions from the other muscles, and that the motor command to pectoralis major capsularis does not change. While the muscle is wrapped around its pulley its length is decreasing linearly, its moment-arm is constant (-0.01 m/rad), and its momvel is zero. The **tension (magnitude of force)** is also decreasing because the muscle force is proportional to the muscle length. Its positive (flexion) torque which is equal to force time moment-arm is decreasing and therefore it is a stable muscle tending to decrease the joint flexion. This stability is shown by the constant negative stiffness.

When the muscle becomes unwrapped ($\theta = 11^{\circ}$) the muscle length and tension continue to decrease but the magnitude of the moment-arm (which is not constant any more) is increasing very fast and the resulting flexion torque is increasing. This causes the muscle to contribute instability to the joint stiffness, as it tends to enhance the flexion. Note that in this case the momvel is negative (a necessary condition for muscle instability) and the angular stiffness is positive (a sufficient condition for instability). At a later stage in the flexion movement (depending on the motor command to the muscle) the flexion torque due to the muscle starts to decrease. At this stage the muscle becomes stable again, and its angular stiffness becomes negative.

9. A NEW GEOMETRIC MODEL

Stability analysis similar to the one done to pectoralis major capsularis in Fig. 6 was done to all the 17 muscles. The results indicate that many muscles have joint angles in which, when the motor command is high, their angular stiffness is not stable. This results in the unstable hand stiffness shown in Fig. 5. This is not a biologically possible situation, as the hand was shown to be mechanically stable even in deafferented monkeys (Bizzi et al. 1982; Taub et al. 1975). Although it is theoretically possible that the CNS will try to choose in such a case only those motor commands which would ensure postural stability, it is not easy (or always possible) to implement such an algorithm. The backdriving algorithm, used in the current computer simulation, assumes that the summation of the angular stiffnesses of all contributing muscles

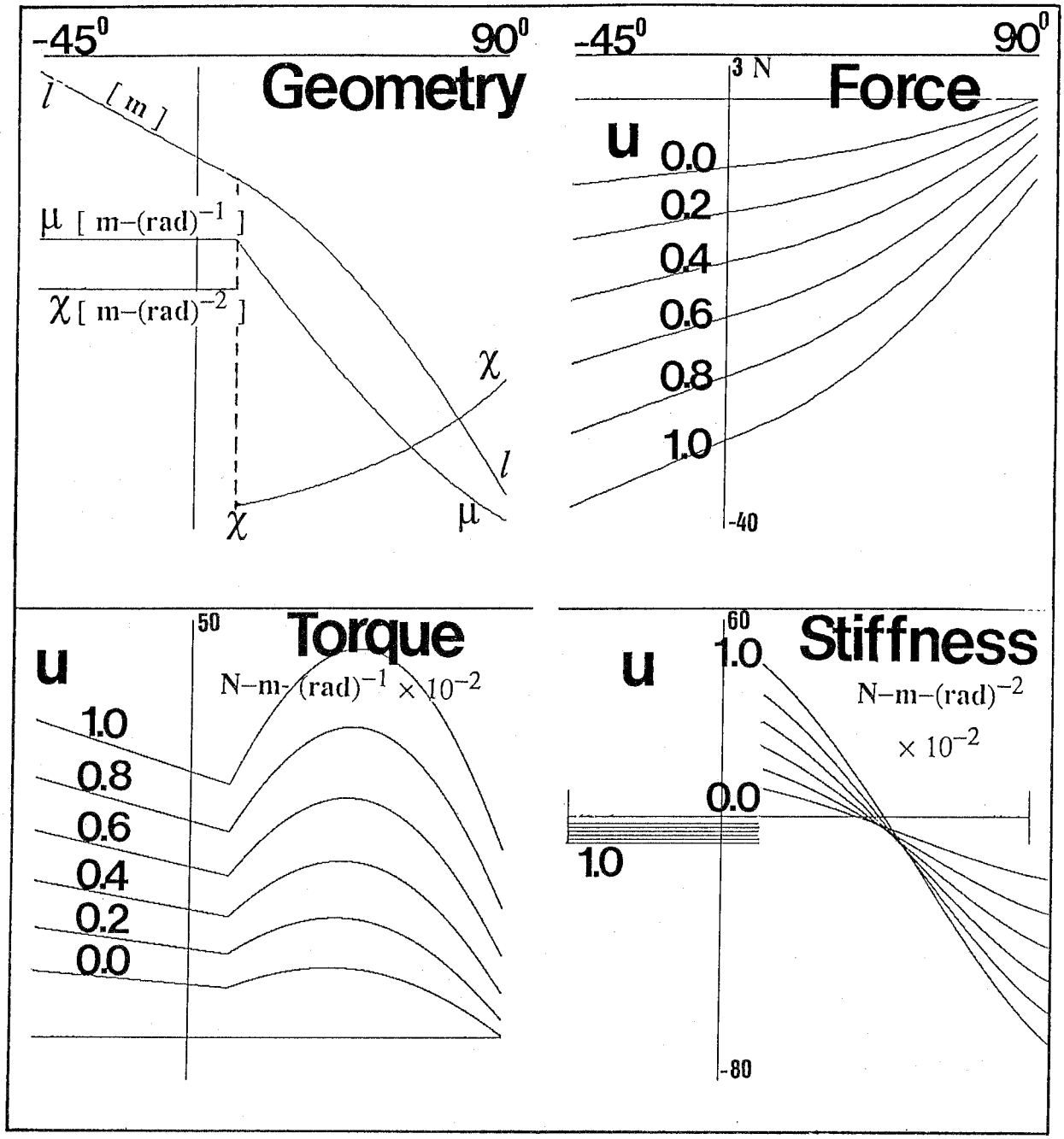

Fig. 6. Stability analysis of pectoralis major capsularis. A flexion movement is shown in which the shoulder angle changes from –45° to 90°. In the **Geometry** panel (upper-left), the muscle length, l, decreased from 0.087 to 0.048 m. The moment arm of the muscle around the shoulder joint, μ, was initially constant at -0.01 $m \cdot rad^{-1}$, but at θ = 11° it started to decrease, eventually reaching its final value of -0.029 $m \cdot rad^{-1}$. The momvel χ was zero at the 1st stage of the movement, jumped to -0.018 $m \cdot rad^{-2}$ at θ = 11°, and then started to increase reaching a final value of -0.0075 $m \cdot rad^{-2}$. In the **Force, Torque** and **Stiffness** panels, the behavior of the muscle is shown for six different motor commands u. From geometrical analysis the muscle can have unstable angular stiffness in θ ∈ [11°, 90°] because in this range χ < 0. Statics analysis, investigating its angular stiffness, shows that it must have unstable angular stiffness in θ ∈ [11°, 40°] and must have stable angular stiffness in θ ∈ [–45°, 11°]∪[48°, 90°].

always defines a stable joint stiffness. If I accept this assumption, how can we achieve that desired situation, without throwing away the linear length tension curves and the biological measurements ?

Looking at the geometric model of the muscles, shown in Fig. 4A for pectoralis major capsularis, a significant simplification is that muscles go directly from origin to insertion. This creates unrealistic muscle geometries, with huge moment-arms and negative momvels. In real biological arms, connective tissues constrain the line of action of the muscles. This can be modeled as frictionless tethereds between the center of attachments of the muscles to the bones and the joints, through which the muscles must pass. If the "effective" origins and insertions which corresponds to those tethereds will fall exactly on the "pulleys" located around the joints (see Fig. 4A), the muscles will have constant moment-arms and their angular stiffness will always be stable. This is not a desired geometry because in real biological arms the moment-arms of many muscles are not constant and vary considerably as a function of joint angle (Amis et al. 1979; An et al. 1981; van Zuylen et al. 1988). As a compromise and a best guess, I estimated and added effective origins and insertions to the muscle geometries (effective origins and insertions were not measured in this study). The heuristic approach employed for estimating the effective origins and insertions is described in Appendix C.

A new, more complex (and more realistic) arm geometry was created. Adding an effective origin and insertion between the measured (center of) attachment and the joint increased the angular stability of the individual muscles. The new geometry chosen for pectoralis major capsularis is shown in Fig. 4B. The coordinates for the effective origins and insertions were calculated to ensure the joint stability for every possible neural control input.

10. ARM MOVEMENT FROM POSTURE

A variety of arm movements between a broad range of different positions in the workspace were produced, using the minimum-jerk model for planning the desired trajectories and the backdriving algorithm for choosing the motor command inputs. A typical movement is shown in Fig. 7.

11. DISCUSSION

Using an analysis by design approach, a simplified model of the arm with muscles extending from origin to insertion was created. Following the design, stability analysis gave insight into the consequences of this design. The instability associated with the initial simplified model was solved by designing a more complex arm in which effective origins and insertions restrained the line of actions of the muscles. Interestingly, the purely **functional** considerations resulted in a more realistic **structure** of the

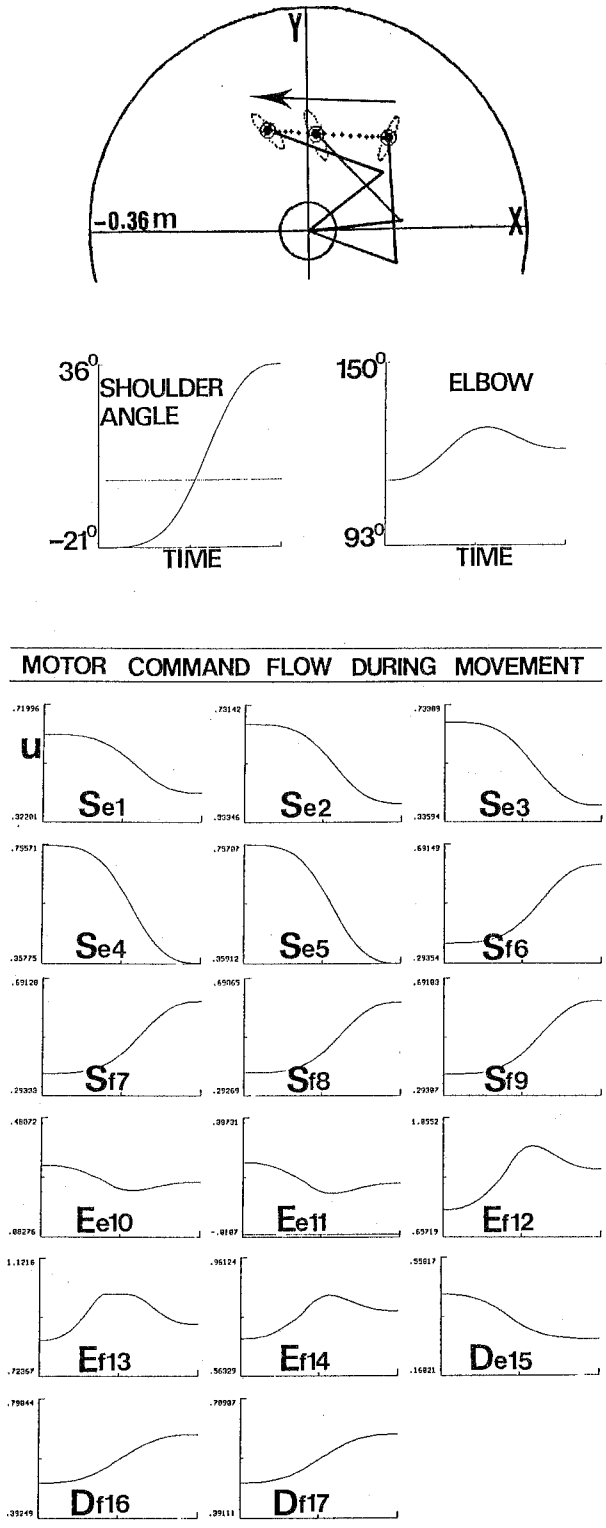

Fig. 7. A typical equilibrium-point movement is simply a gradual shift of the hand along a set of stable intermediate equilibrium points from the initial to the final positions. The trajectory predicted by the minimum-jerk model is a straight line with 26 intermediate points defining a bell-shaped velocity profile. A neural control input to the 17 muscles is specified for each intermediate point, defining it as an equilibrium point. The neural control input profiles for all the muscles is very smooth. When the motor command to a muscle reaches a minimum (0) or a maximum (1), it stays there as long as the backdriving algorithm expects it to decrease or increase, respectively. In this case other muscles take over and produce the needed change in torque. The 13th muscle shows this behavior in the middle of the movement. **S** = shoulder, **E** = elbow, **D** = double joint muscle, **e** = extensor, **f** = flexor. The serial muscle numbers refer to Table 1 and Table 2.

arm. Similar function-structure relationships could affect the evolution process in which the structure of the primate arm was selected.

It is not known whether real biological muscles can have unstable angular stiffnesses. Most of the studies concerning hand stability ignored that possibility, probably because they considered only muscles with constant moment-arms (Flanagan et al. 1990; Flash 1987; Hogan 1985). It was shown by a few studies (Amis et al. 1979; An et al. 1981; van Zuylen et al. 1988) that muscles with varying moment-arm are common for the human arm, and this is also my intuitive impression for the monkey. Using the linear length tension curve assumed in this model, a muscle with a constant moment-arm must have a stable angular stiffness because its momvel is by definition 0, while a necessary condition for angular instability is that the momvel should be negative. The current study is therefore more realistic and revealing from the geometrical point of view compared to previous studies.

When some muscles contribute instability, the joint can remain stable, because only **summation** of the angular stiffnesses of all contributing muscles will determine the joint stability. In our case, shown in Fig. 5, using the initial geometric model, the summation of angular stiffness caused instability in a broad range of the hand workspace. Using a more complex and realistic geometric model, individual muscles may have unstable angular stiffnesses but the joints are stable for any possible motor commands to the muscles.

Increasing the motor commands to an unstable muscle, will increase its contribution of instability. Theoretically, this may make incorrect the assumption (Hogan, 1984) that coactivation is always a simple way to increase the hand stability.

Even if individual muscles can contribute instability to the joints it is still possible that in the real biological arm the summation of the angular stiffnesses is always negative, and therefore the joints are always stable, regardless of the motor commands to the muscles. However, if the summation may become unstable, then the CNS should choose only those neural inputs which ensure joint stability. This would increase the flexibility and complicate the control of hand impedance.

This work is the 1st implementation of the backdriving algorithm (Mussa-Ivaldi et al. in press), describing the control of movement from posture and using a detailed planar model of the primate arm with 17 muscles, according to the principles of the equilibrium point hypothesis. A typical arm movement is shown in Fig. 7. Given the initial motor commands to the 17 muscles, and a final desired hand position and force, the forward arm model calculates the initial hand position and stiffness, the minimum-jerk model specifies the desired trajectory, and the backdriving algorithm calculates the flow of motor commands to the muscles and the driving force to move the hand along the desired trajectory. The final motor command specifies the final hand position, hand force, and hand stiffness. No direct control of the final hand stiffness is present in the current model, and I intend to address this question in a later work.

A disadvantage of the simulator is that it has no memory of previous computations.

Determining the desired trajectory using the minimum-jerk model is instantaneous, but the laborious backdriving algorithm takes about one hour for each trajectory. In order to overcome the essence of this problem, a fast learning, tree-structured network (Sanger, in press) was trained to remember the knowledge obtained by the backdriving algorithm. (Dornay and Sanger, in preparation).

I would like to emphasize that this study is based only on kinematic and static analysis. It does not discuss the dynamics of the arm, and its role in the control of hand stability (Flanagan et al. 1990; Flash 1987).

12. ACKNOWLEDGMENTS:

This work was initiated during my study at MIT, USA, as a Postdoctoral Fellow of Dr. E Bizzi. The theoretical aspects of the work were completed during my study as an invited researcher at ATR Japan. I would like to thank Drs. E Bizzi, FA Mussa-Ivaldi, J McIntyre, Dept. Brain & Cog. Sci., MIT, and Drs. M Kawato, K Nakane and E Yodogawa, Cognitive Processes Dept., ATR, for their valuable help and support. Special thanks are devoted to Dr. M Kawato for his useful comments and proof-readings. Supported at MIT, USA by M. DORNAY NIH Grant, 1-F05-TWO4042-01 and by a MIT Fairchild Fellowship, and at Japan by ATR.

REFERENCES

Amis AA, Dowson D, Wright W (1979) Muscle strengths and musculoskeletal geometry of the upper limb. Engng Med. **8** :41-48.

An KN, Hui FC, Morrey BF, Linchield RL, Chao EY(1981) Muscles across the elbow joint: A biomechanical analysis. J. Biomechanics **14** :659-669.

Berringer OM Jr., Browning FM, Schroeder CR (1968) **An Atlas and Dissection Manual of the Rhesus Monkey Anatomy.** Florida, Anatomy Laboratory Aids.

Bizzi E, Accornero N, Chapple W, Hogan N (1984) Posture Control and Trajectory Formation during Arm Movement. J. Neuroscience **4** :2738-2744.

Bizzi E, Mussa-Ivaldi FA, Hogan N (1986) Regulation of multi-joint arm posture and movement. Progress in Brain Res. **64** :345-351.

Dornay M, Consi T, McIntyre J, Mussa-Ivaldi FA, Bizzi E (1989) A biomechanical model of the monkey's arm. **19th Meeting Int. Soc. Neurosci.** Abstract 26.4.

Dornay M (1990) Control of movement and the postural stability of the monkey's arm, **3rd Int. Symp. on Bioelectronic and Molecular Electronic Devices**, Dec. 18-20, Kobe, Japan :101-102.

Dornay M (1991) Control of movement, postural stability and muscle angular stiffness - A 17-muscle model of the monkey's arm. **IEICE Neuro - Computing**

Meeting, March 18-19, Tokyo, Japan :225-230.

Dornay M, Sanger TD, Control of a monkey arm simulator using a tree-structured artificial neural network. (In Preparation).

Feldman AG (1966) Functional tuning of nervous system with control of movement or maintenance of a steady posture. III. mechanographic analysis of the execution by man of the simplest motor task. Biophysics **11** :766-775.

Feldman AG (1986) Once More on the Equilibrium Point Hypothesis (λ model) for Motor Control. J. Motor Behavior **18** :17-54.

Flanagan JR, Ostry DJ, Feldman AG (1990) Control of human jaw and multi-joint arm movements. In G Hammond (Ed) **Cerebral Control of Speech and Limb Movements**. Elsevier Science Pub., Holland :29-58.

Flash T, Hogan N (1985) The coordination of arm movements: An experimentally confirmed mathematical model. J. Neurosci. **5** :1688-1703.

Flash T (1987) The control of hand equilibrium trajectories in multi-joint arm movements. Biol. Cybern. **57** :257-274

Gray H (1959) **Anatomy of the Human Body**. 28th ed, Philadelphia: Lea and Febiger.

Hartman CG, Straus WL Jr. (1933) **The Anatomy of the Rhesus Monkey**. New-York, Hafner Publishing Co.

Hogan N (1984) Adaptive control of mechanical impedance by coactivation of antagonist muscles. IEEE Transactions on Automatic Control **AC-29** :681-690.

Hogan N (1984a) An organizing principal for a class of voluntary movements. Journal of Neuroscience. **4** pp:2745-2754.

Hogan N (1985) The Mechanics of Multi-Joint Posture and Movement Control, Biol. Cybern. **52** :315-331.

Johnson LW, Riess RD, Arnold JT (1989) **Introduction to Linear Algebra**. Addison-Wesley Publishers, 2ed edition.

McIntyre J, Mussa-Ivaldi F, Bizzi E (1989) Modeling of multi-joint motor systems. Proc. Ann. Int. Conf. IEEE Eng. in Med. and Biol. Soc. **11** :242-243.

McIntyre J (1990) **Utilizing Elastic System Properties for the Control of Posture and Movement**. Ph.D. Thesis, Dept. of Brain and Cognitive Sciences, MIT.

Morasso P (1981) Spatial control of arm movements. Exp. Brain Res. **42** :223-227.

Mussa-Ivaldi FA, Hogan N, Bizzi E (1985) Neural, mechanical and geometric factors subserving arm posture in humans. J. Neurosci., **5** :2732-2743.

Mussa-Ivaldi FA (1986) Compliance. In **Human movement understanding**. P. Morasso, Tagliasco V (Eds.) North-Holland, Amsterdam :159-212.

Mussa-Ivaldi FA, Morasso P, Hogan N, Bizzi E, Network models of motor systems with many degrees of freedom. In **Advances in control networks and large scale parallel distributed processing models**, M.D. Fraser (Ed.) Albex Publ. Corp., in press.

Ogata K (1970) **Modern Control Engineering**. Hall Electrical Engineering Series, Prentice-Hall, Inc., Englewood Cliffs, NJ.

Rack PMH, Westbury DR (1969) The effects of length and stimulus rate on tension in isometric cat soleus muscle. J. Physiol. **204** :443-460.

Sanger TD A tree-structured adaptive network for function approximation in high-dimensional spaces. IEEE Trans. Neural Networks, In Press, 1991.

Strang G **Linear Algebra and Its Applications**. Academic Press, New York, 1988.

Taub E, Golberg IA, Taub P (1975) Deafferentation in monkeys: Pointing at a target without visual feedback. Exp. Neurol. **46** :178-186.

Uno Y, Kawato M, Suzuki R (1989) Formation and control of optimal trajectory in human multijoint arm movement - minimum torque-change model. Biol. Cybern. **61** :89-101.

van Zuylen EJ, van Velzen A, van der Gon JJD (1988) A biomechanical model for flexion torques of human arm muscles as a function of elbow angle. J. Biomechanics **21** :183-190.

Zeffiro TA (1986) **Motor Adaptations To Alterations In Limb Mechanics**. Ph.D. Thesis, Dept. of Brain and Cognitive Sciences, MIT.

APPENDIX A: Estimation of muscle stiffnesses and rest-lengthes.

The following values were obtained for the reference muscle, using data reported by Zeffiro, 1986.

$V^r = 29 \times 10^{-6}\ m^3 =$ volume of reference muscle.

$l^r_{00} = 7.8 \times 10^{-2}\ m =$ rest length of reference muscle when the motor command to the muscle, u, is zero.

$l^r_{01} = 6.3 \times 10^{-2}\ m =$ rest length of reference muscle when $u = 1$.

$\kappa^r_0 = -0.6 \times 10^2\ N \cdot m^{-1} =$ stiffness of reference muscle when $u = 0$.

$\kappa^r_1 = -2.3 \times 10^2\ N \cdot m^{-1} =$ stiffness of reference muscle when $u = 1$.

The following linear function was defined for the reference muscle:

$\kappa^r(u) = (\kappa^r_1 - \kappa^r_0)\ u + \kappa^r_0 =$ the stiffness of the reference muscle.

The following were defined for any muscle:

$l_{00} =$ the rest length of any muscle when $u = 0$. This value was not measured. It was estimated to be 0.99 of the minimum length of the muscle in the workspace. The minimum length of the muscle was calculated, using the measured geometry, by the simulator program. The above estimation assured that the muscles will always have some residual tension, which is very close to zero when the motor command to the muscle is zero, and the muscle is at its minimum length.

$V =$ the volume of the muscle, measured in the dissections.

$$\kappa(u) = \frac{V}{V^r}\left[\frac{l^r_{00}}{l_{00}}\right]^2 \kappa^r = \text{ the stiffness of the muscle.}$$

The above stiffness scaling was proposed by FA Mussa-Ivaldi (personal

communication) and is described in detail in McIntyre, 1990. It is based on the assumption that if muscle sarcomeres each have identical stiffness properties, the stiffness of a muscle is directly proportional to the number of sarcomeres in parallel and inversely proportional to the number of sarcomeres in series. The cross-sectional area provides an estimate of the number of sarcomeres in parralel, while the rest-length corresponds to the number in series (McIntyre, 1990).

$$l_0(u) = \frac{l_{00}}{l^r_{00}} \left[l^r_{01} - l^r_{00} \right] u + l_{00} = \text{ the rest-length of a muscle.}$$

APPENDIX B.

CLAIM:

Given $A = \begin{bmatrix} a & b \\ b & c \end{bmatrix}$ is any real symmetric matrix whose eigenvalues are $\lambda_{1,2}(A)$ then:

$$a < 0, \quad c < 0, \quad ac > b^2 \qquad \longleftrightarrow \qquad \lambda_{1,2}(A) < 0 \tag{B1}$$

PROOF:

Let us define:

$$T = Trace(A) = a+c$$

$$D = Determinant(A) = ac-b^2$$

then following Johnson et al. 1989,

$$\lambda_{1,2}(A) = \frac{T \pm \sqrt{T^2 - 4D}}{2} \tag{B2}$$

Expanding equation (B2) gives us:

$$T = a+c = \lambda_1 + \lambda_2 \tag{B3}$$

$$D = ac-b^2 = \lambda_1\lambda_2 \tag{B4}$$

Since A is a (n x n) real symmetric matrix, then all the eigenvalues of A are real (Johnson et al. 1989), which gives us:

$$T^2 - 4D \geq 0 \tag{B5}$$

Direction 1:

Given $\lambda_1 < 0$ and $\lambda_2 < 0$ **proof that :**

(i) $ac > b^2$

(ii) $a < 0$

(iii) $c < 0$

Proof of Direction 1:

$\lambda_1 < 0\,,\ \lambda_2 < 0 \rightarrow \lambda_1\lambda_2 > 0 \rightarrow D > 0 \rightarrow ac - b^2 > 0 \rightarrow ac > b^2.$
End proof of (i).

$ac > b^2 \rightarrow (a > 0,\ c > 0)$ *or* $(a < 0,\ c < 0)$.
If $a > 0,\ c > 0$ Then $a+c > 0$. But we know that $a+c = \lambda_1+\lambda_2 < 0$.
So we must have $a < 0,\ c < 0$. End proof of (ii) and (iii) .
End Proof of Direction 1.

Direction 2:

Given $a < 0,\ \ c < 0,\ \ ac > b^2$ **proof that :** $\lambda_{1,2} < 0$

Proof of Direction 2:

$$ac > b^2 \rightarrow ac - b^2 > 0 \rightarrow D > 0 \rightarrow 0 > -4D \rightarrow T^2 > T^2 - 4D$$

$$\rightarrow |T| > \sqrt{T^2 - 4D} \quad \text{(remember that } T^2 - 4D \geq 0\text{)} \rightarrow$$

$$T > \sqrt{T^2 - 4D} \quad \text{or} \quad T < -\sqrt{T^2 - 4D}$$

$$\text{but } T = a+c < 0 \rightarrow T < -\sqrt{T^2 - 4D} \rightarrow T + \sqrt{T^2 - 4D} < 0$$

$$\rightarrow T \pm \sqrt{T^2 - 4D} < 0 \rightarrow \lambda_{1,2}(A) = \frac{T \pm \sqrt{T^2 - 4D}}{2} < 0.$$

End Proof of Direction 2.

APPENDIX C: Estimation of effective origins and insertions.

The following is an heuristic approach for substituting lacking biological parameters about the effective origins and insertions of the muscles. While the estimations obtained do create a stable arm geometry, those values should not be considered as true replacements to real biomechanical measurements.

Fig. 1C describes a muscle affecting a joint **O**. The muscle inserts on the link $\overline{\mathbf{O}\text{–}\mathbf{X}}$. The coordinates of the insertion are **(c,d)**, and the distance from the joint to the insertion is **P**. The radius of the pulley of this muscle around the joint (Fig. 4A) is **R**. The line connecting **O** to **P** transverses the pulley at coordinates **(a,b)**. I assume for simplicity that the effective insertion is located on the line segment between **(a,b)** to **(c,d)**.

The following nomenclature is used to describe the coordinates of the effective insertion **Z** on the line $\overline{\mathbf{R}\text{–}\mathbf{P}}$.

1. If the effective insertion falls on **P**, the initial muscle geometry, shown in Fig 4A, is produced. This case is marked as 100%, and indicates the most unstable geometry.
2. If the effective insertion falls on **R**, the most stable geometry, marked as 0%, is produced.
3. In the general case the effective insertion falls on a point **Z**, and this is described as **(Z–R)/(P–R)**×100 percent.

I assume for simplicity that the same "percent" is applied both to the effective origin and to the effective insertion.

A stable geometry could be found for each of the 17 muscles by changing its effective geometry in small steps from 100% to 0%, and measuring the corresponding muscle angular stiffnesses while the motor command to the muscle is $u = 1.0$. Usually, the effective geometry closest to 100% in which the muscle was stable in all the workspace, was chosen. For example, an effective geometry of 15% guarantied the stability of pectoralis major capsularis for any motor command and any joint angle in the hand workspace (see Fig 4B). I should emphasize that this is the maximal requirement, for the highest possible motor command and in all the workspace. Brachio-radialis was chosen intentionally as an exception, and its chosen effective geometry (75%) allowed it to be unstable in about half of the elbow workspace.

The following effective geometries were chosen for the 17 muscles: latissimus dorsi, 15%; posterior deltoid, 5%; teres major, 10%; teres minor, 100%; infraspinatus, 100%; pectoralis major capsularis, 15%; pectoralis major sternalis, 10%; anterior deltoid, 25%; coracobrachialis, 45%; triceps lateralis, 90%; triceps medialis, 100%; brachialis, 15%; brachio-radialis, 75%; pronator teres, 40%; triceps longus, 0.001%; biceps brevis, 0.001%; biceps longus, 0.001%. This geometry

ensures the joint stability, and hand stability at equilibrium, for every possible motor command and hand position in the workspace.

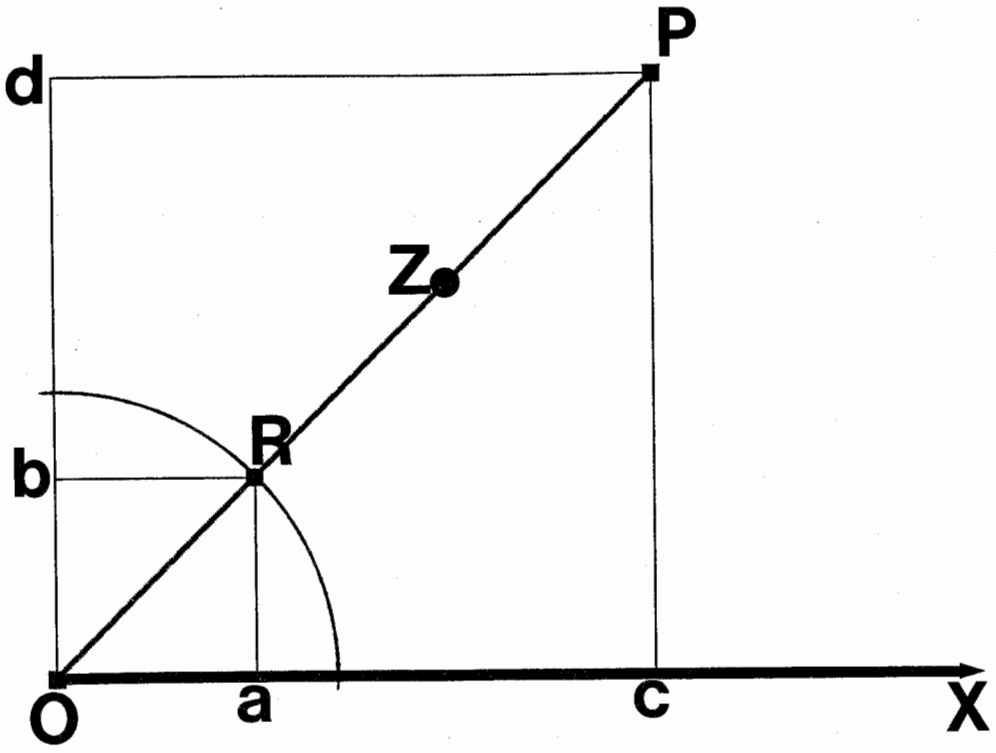

Fig. 1C. The geometrical location of an effective origin or an effective insertion of a muscle. Please refer to the text of Appendix C for explanation of this figure.